Fusion Engineering and Design 144 (2019) 193–201

Contents lists available at ScienceDirect

Fusion Engineering and Design

journal homepage: www.elsevier.com/locate/fusengdes

High-directional laser-plasma-induced X-ray source assisted by collimated electron beams in targets with a self-generated magnetic field

Huan Li[a,b], Xiaobin Tang[a,c,*], Shuang Hang[a], Yunpeng Liu[a,c], Junxu Mu[a], Wei Zhou[a]

[a] Department of Nuclear Science and Engineering, Nanjing University of Aeronautics and Astronautics, Nanjing 211106, China
[b] Institute of Laser Engineering, Osaka University, Suita, Osaka 565-0871, Japan
[c] Key Laboratory of Nuclear Technology Application and Radiation Protection in Astronautics, Nanjing 211106, China

GRAPHICAL ABSTRACT

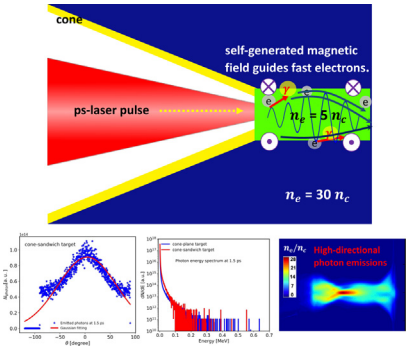

ARTICLE INFO

Keywords:
Laser plasma X-ray source
Fast electrons
Self-generated magnetic field
Particle-in-cell simulation
Synchrotron radiation process

ABSTRACT

Advances in ultra-intense laser pulse and plasma diagnostic technologies have fostered tremendous progress in the high-performance X-ray photon source. In this paper, we proposed a novel cone-attached sandwich target with a sharp density gradient, which can guide and reflect much laser pulse to the target, to get a high-directional and micro-sized laser-plasma-induced X-ray source with a smaller divergence angle and higher brilliance. 2D PIC simulations were performed to investigate the laser-plasma-induced X-ray photon emissions in the proposed target at a laser intensity of 2.5×10^{20} W/cm^2. Results indicated that most of the high-directional photons were radiated by the forward-moving fast electrons. Although the accelerated electrons will experience slightly transverse oscillations due to the electric field of the laser pulse, they will be guided and confined by the self-generated magnetic field (311 MG) along the interface of the proposed target, and then the divergence angle of the fast electrons can be deceased as well. These underlying mechanisms enhance the X-ray photon emissions in the proposed target, which show a promising application in high energy density physics and inertial confinement fusion field.

1. Introduction

Laser plasma interactions have attracted much interest from fundamental science to practical applications [1] because of the rapid development of ultra-intense and ultra-power laser technology, advanced plasma target fabrications and diagnostic facilities [2]. What

* Corresponding author at: Department of Nuclear Science and Engineering, Nanjing University of Aeronautics and Astronautics, Nanjing 211106, China.
E-mail address: tangxiaobin@nuaa.edu.cn (X. Tang).

https://doi.org/10.1016/j.fusengdes.2019.05.001
Received 19 December 2018; Received in revised form 30 April 2019; Accepted 2 May 2019

significantly attracts many researchers is the generation of high-directional X-ray photon source with high brilliance and small divergence angle due to the critical roles it plays in many potential applications. For example, a hard X-ray or γ-ray source with a high-intensity ($> 10^{10}$ photons), short pulse duration time (fs ~ ps), broad energy spectrum (up to MeV) and small source size with several μm becomes desirable as usual to diagnose the non-equilibrium and transient plasma in high energy density (HED) condition [3,4]. Hard X-ray radiographic snapshots of cold dense DT fuel in inertial confinement fusion (ICF) was employed to probe the implosion targets, and the technology was based on the point-projection radiography which needs a broad photon energy range from 60 to 200 keV and smaller source size (several μm) [5]. High brilliance of 500–1000 keV X-rays was also required to realize the optimum image contrast for non-destructive testing application in nuclear waste packages [6] and advanced materials measurement techniques [7], considering X-ray transmission properties from the NIST database tables [8]. The development of high brilliance X-ray source is also crucial for microbeam radiation therapy to decrease acquisition times at high spatial resolution [9,10], and this approach employed planar μm-width X-ray beam arrays with high radiation doses of several hundred Grays. Additionally, a modulated X-ray source, with a broad photon energy spectrum (~ several hundred keV) and small divergence angle because of different reentry altitudes and signal losses, is an important component for effective X-ray communication [11], which would be expected to mitigate blackout communication during spacecraft reentry and provide a high data rate with ground station [12].

Although a conventional X-ray tube is a cheap and flexible source for these applications, the extremely low conversion efficiency from the accelerated electrons to the emitted X-ray photons (~ 1%) with a large photon emission divergence and low radiation brilliance will limit its application in these sophisticated research fields. Thus far, there existed some X-ray generation mechanisms. For example, the conventional synchrotron radiation facilities [13,14] are hard to extend the radiation energy to MeV because of the dielectric breakdown of materials, and its large-scale size and cost-consuming properties also limit the would-be users. Recently, the all-optical inverse Compton scattering X-ray source [15] becomes an intriguing alternative to synchrotrons, but its application is still restricted due to the limited photon energies and field size. Considering the X-ray attenuation in high-Z materials is high, it will not suitable for some particular occasions such as the nuclear waste containers monitoring. Although the betatron radiation source has a narrow divergence angle of photon emission, the photon yield is still relatively low for HEDS because of the low charge electron beams [16,17]. Currently, high-intensity laser interactions with plasma target would generate a novel regime of the X-ray photon emissions through the nonlinear synchrotron radiation, which attracts much attention among a wide range of analytical and experimental studies [18–21]. Laser-plasma-induced X-ray sources will feature the high performance photon emissions, such as the enhancement of energy conversion efficiency, higher photon flux, and peak brilliance compared with the conventional X-ray sources, making possible the realization of table-top X-ray source. Multi-scale theoretical simulations accompanying the experiments clearly [22] illustrate that the divergence angle and focused spot size of the emitted photon emissions are so large that we cannot acquire much brighter and high-directional X-ray radiation source. However, in the current literature little attention has been paid to the relation of the emitted X-ray photons radiated by the fast electrons, and also the deeper insight into the photon's collimation (angular distribution) controlled by the guiding effects of the fast electrons under the laser's electric field-induced strong transverse oscillations and the self-generated magnetic field confinement.

In this paper, we proposed a special-structured (cone-sandwich) target with a number density gradient which can significantly reduce the divergence angle and transverse size of the emitted X-ray photon emissions, followed by a detailed description of the underlying mechanisms in the laser-irradiated plasma target by using 2D Particle-In-Cell (PIC) simulations. Results shown that for the cone-sandwich target most of the X-ray photons were radiated by the fast electrons with the forward-moving directions in the synchrotron radiation process compared with the cone-plane target. However, we discovered that the high-directional X-ray emission source with high brilliance was enhanced by another important mechanism simultaneously. Although the fast electrons were accelerated and oscillated in the transverse direction due to the electric field of the laser pulse, a kT-level self-generated magnetic field along the interface of the target density gradient played a significant role in confining and guiding the fast electrons transport, strengthening the directionality of the photon radiations with high brilliance and wide energy range. Compared with the cone-sandwich target, the cone-plane target (for comparison) emitted an undirected photon beam with large divergence angle and scattered fast electron transport without self-generated magnetic field.

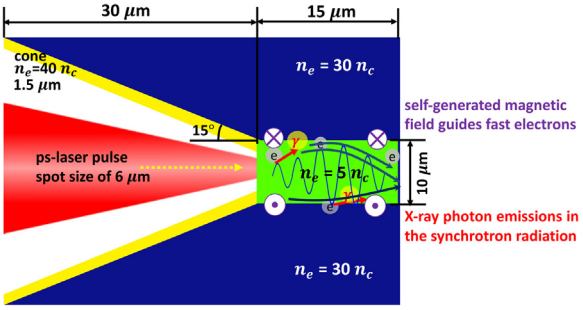

Fig. 1. Schematic diagram the cone-sandwich target, the principles of fast electrons guiding and X-ray photon emissions in the synchrotron radiation driven by an ultra-intense laser pulse interaction with the plasma target. For comparison, the reference cone-plane target with the same size is also studied, but all the carbon number density is $5n_c$, where n_c is the critical density for 1 μm laser wavelength.

2. Theories and methods

As illustrated in Fig. 1, we proposed a novel cone-attached sandwich target to get the high-directional laser-plasma X-ray source. The target consisted of a 30 μm-long hollow open-tip copper cone connecting with a 15 μm-long vitreous carbon sandwich layers with different number densities. The thickness of the cone is 1.5 μm, and its open-tip angle is 30°. The 5 μm middle transport channel radius was chosen to match the laser's spot size and optimize laser coupling into the channel. The simulations were carried out by the relativistic parallel 2D-PIC EPOCH [23] code in a region of 50 μm × 40 μm whose cell size was 10 nm × 10 nm with 58 electron macroparticles, 10 copper and 20 carbon ion macroparticles per cell. The boundary conditions for the simulations are periodic in the *y*-direction and open in the *x*-direction. To reduce the numerical heating due to the restrictions on the grid size compared with Debye length, the simulations were performed using a fourth order spline interpolation for particle weightings. A p-polarized Gaussian laser pulse with the wavelength (λ) of 1.0 μm and the duration (τ) of 1.5 ps in FWHM propagated from the left boundary to the right. The laser had a maximum intensity of 2.5×10^{20} W/cm^2 in the y direction with a FWHM spot size (w_0) of 6.0 μm. The laser was incident normally on the middle carbon layer surface and kept on for the entire duration of the simulations. The initial ionization charge state for copper was set to +4, and we initialized the sandwich parts as fully ionized carbon plasma with different electron densities ($5n_c$ in the middle layer, and $30n_c$ in the top and bottom layers), which in practice correspond to foam (low-density)/plastic (high-density) target or plastic (low-density)/aluminum (high-density) target. Here n_c was the critical density (at which the plasma frequency equals the frequency of an electromagnetic wave through a plasma). In order to explain the advantageous properties of the suggested configuration on the high-

directional X-ray emissions, we also investigated the cone-plane target for comparison. The target was fabricated with the same size of the copper cone and the uniform carbon density of $5n_c$. Enhanced Multi-MeV photon emissions as a function of target density were revealed by considering the ultra-intense laser intensities up to 10^{22} W/cm^2 [24]. The front surface of carbon middle layer is preceded by a 4 μm-long exponentially decaying density profile varying from $0.01n_c$ to $5n_c$ with a $1/e$ scale length of 1 μm in order to increase the interaction time of the laser with the under-dense pre-plasma.

The nonlinear synchrotron emission is regarded as the primary source of X-ray photons in the quantum electrodynamic (QED) effects [25,26]. The formation length of the photon emission and pair production is much less than the scale of variation of the field in most cases because the QED processes are usually only important for a laser strength parameter (or normalized laser amplitude) $a_0 \gg 1$, where $a_0 = \sqrt{\frac{e^2(I\lambda^2)}{2\pi^2 c^5 \epsilon_0 m_e^2}} = \sqrt{\frac{(I\lambda^2)}{1.37\times10^{18}}}$ (ϵ_0 is the vacuum permittivity, and $I\lambda^2$ is the normalized laser intensity). This parameter also estimates whether the electron motion oscillating in the laser's electromagnetic field is in the relativistic regime. The relativistic EPOCH code we employed in the study has implemented QED subroutine which can be used for pair production, synchrotron emission and radiation reaction studies during the laser-plasma interaction [23]. The code contains a probabilistic method based on the classical and QED synchrotron cross section to calculate the hard X-ray photon emissions [26]. Note that, for investigating the photon emission distributions radiated by the fast electrons, we calculated the generation points of the emitted photons with energies higher than 10 keV in the current simulations, and their motions through the domain were not simulated and then they stayed where they were generated. In addition, we adopted cone-attached structure for the following reasons [27]. First, the ultra-intense laser light is reflected at the side wall of the cone, guided into the tip of the cone and eventually most of the laser energy is deposited into the cone tip [28] for the purpose of experiment. Also, it avoids the difficulty of laser-driven hole boring into overcritical density plasma with laser pulse. Final, it can prevent potentially deleterious laser interaction with coronal plasma which will affect the incidence laser's properties in the ICF field [29]. For a general laser-plasma interaction experiment, it is a common practice to place the target in TCC (Target Chamber Center) position. In this case, a laser with special energy will be compressed to our expected pulse duration by a segmented-grating pulse compression system. The laser pulse will be focused onto the target by an off-axis parabolic mirror in p-polarization with an incident angle [30]. During this process, one or more special diagnostic facilities will be exploited to measure the target position from side/top view to ensure the experiment conducted smoothly.

3. Results and discussions

3.1. Conversion of laser to target and guiding properties of fast electrons

The cone-sandwich target with number density gradient and the cone-plane target with uniform number density were employed to examine the distribution of fast electrons and the emitted photons. For all the simulations, we defined electron with a Lorentz factor of $\gamma \geq 1.3$ (corresponding to 150 keV) as fast electron, and the electron with $\gamma < 1.3$ as bulk or background electron. That is, 150 keV in the simulations is used as an arbitrary cut-off energy to differentiate the fast and background electron.

Fig. 2 shows the corresponding 2D PIC simulation results of two kinds of targets at 1.5 ps. During laser interaction with plasma target, the laser's Rayleigh range (z_R) is an effective parameter to describe the distance along the propagation direction of a beam from the waist to the place where the spot size increases by a factor of $\sqrt{2}$ and the intensity is decreased by a factor of 2. In the current simulations, the z_R ($=\pi w_0^2/\lambda$) was 28 μm, which was larger than the laser-plasma interaction region size (15 μm). At the beginning of the simulation, the laser intensity was ramped up over 210 laser cycles (T_c = 3.3 fs) to the maximum, after which the laser amplitude was kept constant to the end of the calculation until 1.5 ps. For the cone-plane target with uniform density ($5n_c$), the laser beam propagation in the near-critical transparency regime will experience the severe transverse tilting in Fig. 2(e). As the laser pulse deviates from its axis, so will the fast electrons accelerated and transported by the laser pulse in Fig. 2(d). Since photons are essentially emitted almost parallel with these fast electrons momentum during the synchrotron radiation process, the direction of the photon beam also becomes unstable and is deflected along with the turning trajectories of the fast electrons, as indicated in Fig. 2(f). However, the titling behavior of the laser pulse propagation and the scattering effect of the fast electrons are suppressed in Fig. 2(b) and 2 (a) by employing the proposed cone-sandwich target with density gradient from $5n_c$ (inner region) to $30n_c$ (outer region). This leads to an extremely high degree of collimation for photons, as illustrated in Fig. 2(c). Therefore, the tilted laser's wavefront was modified by the number density gradient, the intense laser was well guided, and the fast electrons are directed along the channel axis. Accordingly, a stable and high-directional X-ray photon beam is generated along the laser incident axis in Fig. 2(c) compared with the cone-plane target. In the following we discussed the fast electrons properties during the laser interaction with the targets. Calculations of laser-to-fast electrons conversion efficiency ($\eta_{L\rightarrow f}$) in EPOCH were considered by taking the ratio between the total energy of all fast electrons and the total laser pulse as given [23]:

$$\eta_{L\rightarrow f} = \frac{1}{E_{\text{laser}}} \sum_{j=1}^{N} n_j \times w_j \times E_j, \tag{1}$$

where E_{laser} is the total laser pulse energy, n is the number of macro-particles with relevant weight (w) and energy (E).

During laser interactions with plasma, a population of fast electrons will stream out from the plasma in the backward direction and another in the forward direction. It has been proved that the angular distribution of the fast electrons begins to increase drastically if the laser intensity is above 10^{18} W/cm^2 [31]. In the current simulations, the divergence angle (θ) of the electrons above 150 keV ($\gamma \geq 1.3$) was derived from the momenta vector (p_x *and* p_y) of the tracked electrons. Fig. 3(a) shows the angular distribution of the fast electrons streaming out of the plasma in the forward direction and the corresponding Gaussian fits with $f(\theta) \sim \exp(-\frac{\theta^2}{2\sigma^2})$ [32] of the cone-sandwich target, and the parameter σ was fitted to be 45.1° and 47.1° for the forward-moving fast electrons in the cone-sandwich target at 0.8 ps and 1.5 ps. A great deal of fast electrons are trapped in the low-density transport region of the cone-sandwich target (see Fig. 2(a)) and are confined around the laser propagation axis with a relatively smaller divergence angle. However, for the cone-plane target, as indicated in Fig. 3(b), there are several peaks in the fast electrons angular distribution relative to the laser's initial propagation axis at 0.8 ps and 1.5 ps. This means the high-energy fast electrons are distributed asymmetrically and deflected in a wide range of the transverse directions (see Fig. 2(d)).

As laser pulse propagates the target, laser's energy will be converted into the fast electron energies and the relevant radiation processes by either relativistically induced transparency [33] in the lower densities (pre-plasma) or stable hole boring effects [29] in the higher densities. Fig. 3(c) shows the total fast electrons energy as a fraction of the energy which has entered the system by the laser pulse for two targets. In all of the performed simulations, approximately 60% and 35% of the incident laser energy has been transferred to the fast electrons and the forward-moving fast electrons (with a positive p_x) for the two targets. This is in good agreement with previous work by Ping et al in which the total absorbed laser energy was investigated with different laser intensities [31]. The slow increase in absorption curve after 1.1 ps simply depends on the time it takes for laser pulse to reach the plasma target. For the

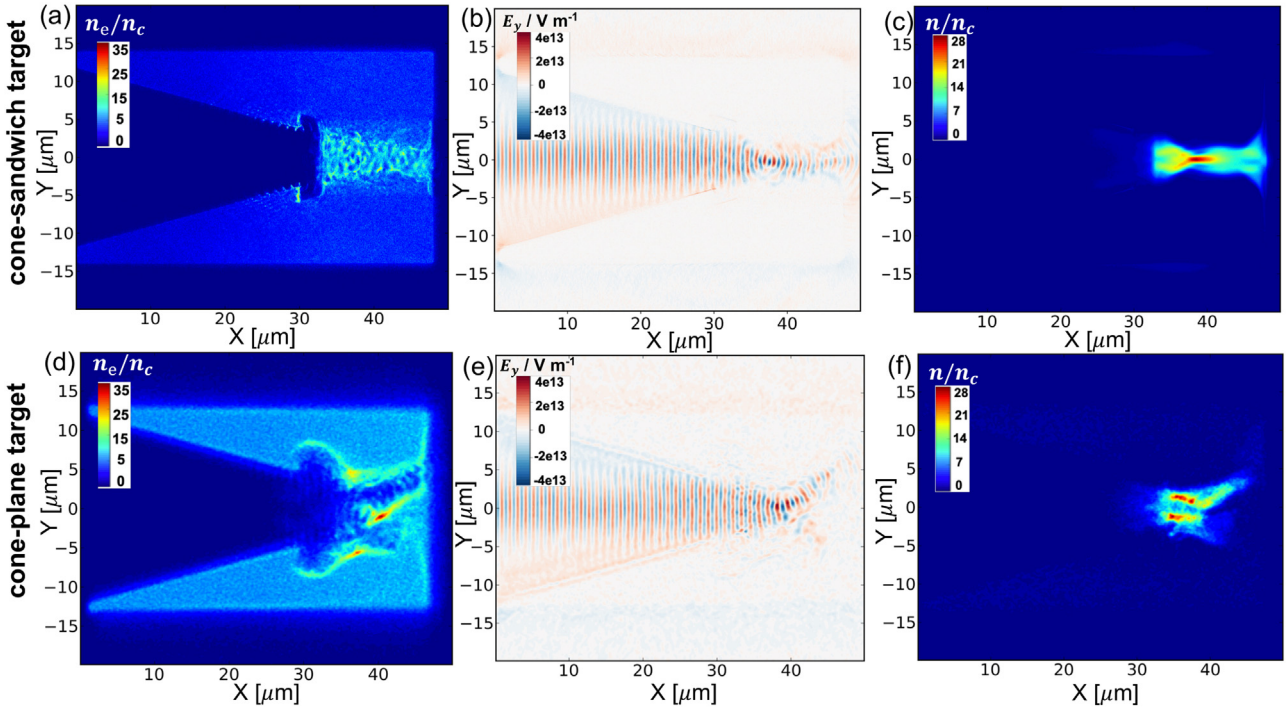

Fig. 2. Results of 2D simulation number density and laser electric field profiles. Number density of the fast electrons ($\gamma \geq 1.3$) at 1.5 ps during laser interaction the proposed (a) cone-sandwich and (d) cone-plane (for comparison) target, which are normalized by the critical density n_c of 1.1 $\times 10^{21}$ cm^{-3} for 1 μm laser wavelength. Panels (b) and (e) show the electric field snapshots of the incident laser for the cone-sandwich and cone-plane target at 1.5 ps, respectively. Number density of the emitted photons with energies greater than 10 keV in the (c) cone-sandwich and (f) cone-plane target at 1.5 ps.

two cases, the maximum value of the number density of fast electrons induced by the laser pulse was approximately at 1.1 ps, which means the more laser energy was converted into fast electrons. The electron energy spectrum has two main components in PIC simulation of a laser-plasma interaction, which are the generated fast electrons and a cold background electrons that remain trapped in the plasma. Characterization of fast electrons involves fitting the slope temperature of high energy tail of the electron energy spectrum which can be described by Maxwellian distribution. That is, $f(E) \sim E^{1/2}\exp(-E/T_h)$, where E is the electron energy (MeV) and T_h is the hot electron temperature (MeV). As shown in Fig. 3(d), the fitted slope temperature for the cone-sandwich and cone-plane target is 4.34 MeV and 4.53 MeV, respectively. The ponderomotive $\mathbf{j} \times \mathbf{B}$ heating scaling law overestimates the slope temperature as $T_h(\text{MeV}) = 0.511[(1 + I_{18}/1.37)^{1/2} - 1]$ of 6.41 MeV [34]. The difference between the calculation fitting values and the scaling law because the law only depends on the laser's strength parameter ($I\lambda^2$) and neglects the comprehensive effects of the fast electron generation, transport and self-generated magnetic field.

3.2. High-directional X-ray photon emission source

We first examined the number density profiles of the emitted photons during laser interactions with the cone-sandwich target in Fig. 2(c) and the cone-plane target in Fig. 2(f), which illustrate that the photon emissions are mainly distributed and collimated in the middle transport region of the cone-sandwich target. The angular distributions of the emitted photons relative to the laser propagation axis were calculated in the middle region of the cone-sandwich target and the whole region of the cone-plane target corresponding to the two different cases. We defined the half spread angle of a photon as $\theta = \tan^{-1}(p_y/p_x)$, where p_x and p_y are the momenta of the tracked photons in the x and y directions in the EPOCH simulations. In general, it is a common practice that the Gaussian function fits the photons' angular distribution in laser plasma interaction field by using the fitting function $f(\theta) \sim \exp(-\frac{\theta^2}{2\sigma^2})$ [32]. Fig. 4(a) illustrates that the emitted X-ray photons of the cone-sandwich target are highly collimated and the angular divergence can be fitted with σ of 45. 5° (FWHM = 107. 1°) from the incident laser axis (0°). It should be pointed out that the proposed target guides the laser pulse so that the emitted photon beam is symmetric and directed along the transportation region channel. However, for the cone-plane target in Fig. 4(b), the radiated photon emissions are off-axis and can be interpreted as two-directional distribution with a large transverse size of fitted σ_1 = 71. 0° (FWHM1 = 167. 3°) and σ_2 = 70. 6° (FWHM2 = 166. 4°) relative to their own peak position at ∓150°. Since the energetic electrons accelerated by the laser pulse essentially emit photons parallel to their momentum, the directivity of the photon beams in Fig. 2(f) becomes unstable or unpredictable with a larger divergence angle compared with the cone-sandwich target. In addition, the radiated energy per photon at 1.5 ps of the two targets in the simulations as a function of the emitting electron longitudinal momentum are investigated in Fig. 4(c). It shows that the most emitted high energy photons are produced by the forward-moving fast electrons ($p_x > 0$) in the cone-sandwich target (red), yet for the cone-plane target (blue) the photons are emitted by both forward-moving ($p_x > 0$) and backward-moving ($p_x < 0$) electrons. These correspond to the divergence angle and number density distribution with the fast electrons in Figs. 2 and 3. That means, the guided fast electrons propagating the cone-sandwich target and scattered fast electrons traveling through the cone-plane target would be the main reason of high-directional or low-directional X-ray photon emissions.

Based on the above discussions, we have discovered that the proposed cone-sandwich target shows a great advantage in the high-directional X-ray emission with a small transverse size compared with the cone-plane target. Additionally, in EPOCH simulations, distribution functions are normalized so that the value at every point of the distribution function is the number of particles within that cell of the distribution function. That is, the number given in the distribution function is the sum of all the particle weights for that particular energy bin. The X-ray photon energy spectrum with a broadband tail, and the cut-off photon has a high energy, although the corresponding photon

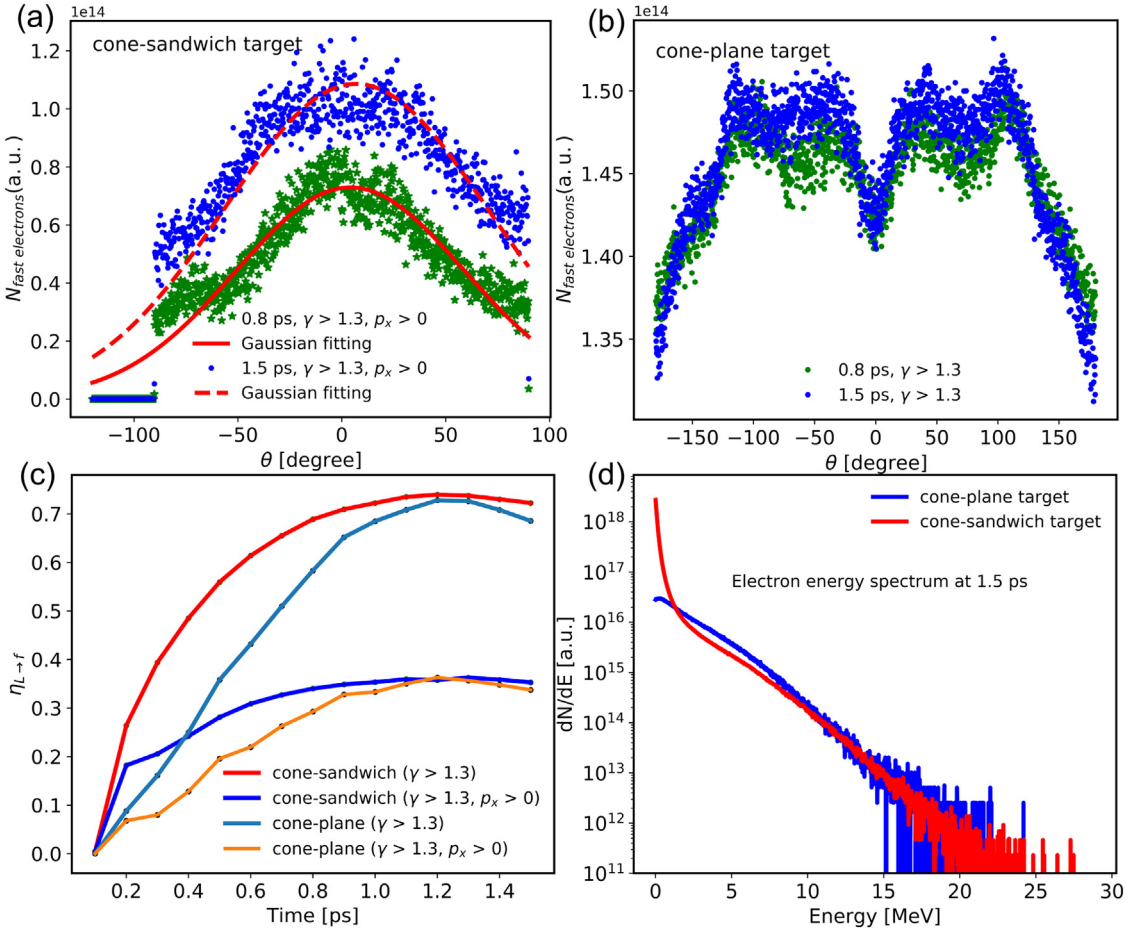

Fig. 3. Properties of fast electrons. (a) Angular divergence distribution of fast electrons ($\gamma \geq 1.3$) and the corresponding Gaussian fits of the cone-sandwich target at 0.8 ps and 1.5 ps, where $\theta = \arctan(p_y/p_x)$; (b) Angular divergence distribution of the fast electrons ($\gamma \geq 1.3$) of the cone-plane target at 0.8 ps and 1.5 ps. The distributions are averaged over domain between the middle transport region for the cone-sandwich target and whole region for cone-plane target. (c) Instantaneous laser-to-fast electrons conversion efficiency. Time evolution of the total kinetic energy of the fast electrons ($\gamma \geq 1.3$) and the forward-moving fast electrons ($p_x > 0$) for the two targets. (d) Electron energy spectrum snapshots at 1.5 ps for the cone-sandwich target (red) and cone-plane target (blue).

number are small. The maximum energy of the emitted X-ray photons would be 250–300 keV for the two targets, as shown in Fig. 4(d). The integrated photon emission numbers with a broad energy spectrum from 10 keV to 300 keV for the cone-sandwich target was about 8.4×10^{13}, which was at least 3 orders higher than that in the betatron radiation [16,35]. If we consider the photon emission source radius of 4.5 μm (the cone-sandwich target), a divergence angle of 0.78 × 0.78 rad^2, a bandwidth of 100%, and a pulse duration of 1.5 ps (same as the laser pulse), this leads to a peak X-ray photon brightness up to 10^{21} photons/s/mm^2/mrad^2/0.1%BW. By estimating every emitted photon's energy and combining its corresponding weight, the energy conversion efficiency ($\eta_{L\to p}$) from laser to the photons was about 4.2% and 3.6% for the cone-sandwich and cone-plane target, respectively. The $\eta_{L\to p}$ is related to the plasma number density, laser intensity, guiding effects of fast electrons, and the strength of the quasi-static magnetic field. Previous studies showed that the conversion efficiency was up to ~15% [19] with the laser intensity of 10^{22} W/cm^2. For the cone-sandwich case, we tried to run the simulation with laser intensity of 9.0×10^{20} W/cm^2 further, the emitted photon's energy could be extended to higher energies of 1–2 MeV.

For the synchrotron radiation process, the photons are emitted almost parallel with the fast electrons momentum. In order to discover the underlying mechanisms for the high-directional X-ray photon emissions of the proposed target, let us consider the instantaneous power radiated by a single fast electron as the following [25]:

$$P = \frac{4\pi m_e c^3}{3\lambda_c}\alpha_f \eta_c^2 g(\eta_c) \propto \eta_c^2, \tag{2}$$

where $\eta_c = \gamma\sqrt{(\mathbf{E} + \frac{1}{c}[\mathbf{v}\times\mathbf{B}])^2 - \frac{1}{c^2}(\mathbf{E}\cdot\mathbf{v})^2}/\mathbf{E}_s$ and $g(\eta_c) \approx [1 + 4.8(1+\eta_c)\ln(1+1.7\eta_c) + 2.44\eta_c^2]^{-2/3}$. $\mathbf{E}$ and $\mathbf{B}$ are the electric and magnetic fields of the laser pulse. $\mathbf{v}$ and $\gamma(=(1-(v/c)^2)^{-1/2})$ are the velocity and Lorentz factor of the electrons. $\mathbf{E}_s \simeq 1.3 \times 10^{18}$ V/m is the Schwinger limit. λ_c is the Compton wavelength, and α_f is the fine structure constant. From Eq. (2) the photon radiations are emitted mainly into a cone-angle, which would be regarded as entirely in the forward direction by considering the fast electrons here. The parameter η_c can be used for effectively estimating the strength of the electric field compared to $\mathbf{E}_s$, and determines the photon's radiation process for an ultra-relativistic electron in a strong electromagnetic field. The laser typically accelerates electrons to $\gamma \sim a_0$ [25], where a_0 is the strength parameter of the laser pulse. Supposing the maximum electric field of the laser, $E_{max} = 3.0 \times 10^{13}$ V/m, derives the $\eta_c = 9.8 \times 10^{-5}$. From the PIC simulations of the two targets, we observed $\eta_c = 1.7 \times 10^{-3}$ for the cone-sandwich target and $\eta_c = 1.2 \times 10^{-3}$ for the cone-plane target by considering the maximum photon's emission power. Note that such high electric field of the laser does oscillate electrons in the transverse direction, and the deflection angle relative to the laser propagation axis is also illustrated in Fig. 3(a) and (b). The parameter η_c is lower than what is derived from the PIC simulation. Therefore, we can conclude that it should exist another mechanism to influence and enhance the X-ray photon emissions in the real physical process. In addition, we

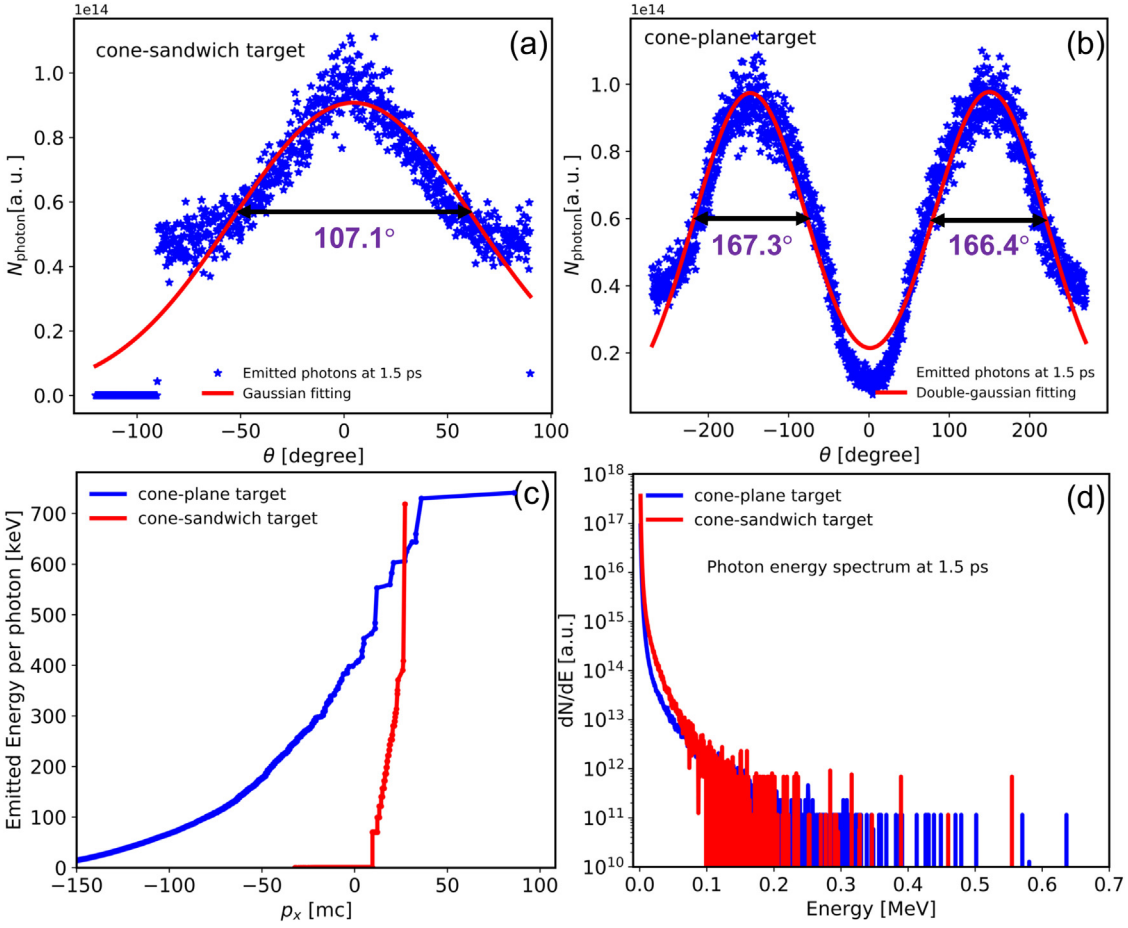

Fig. 4. Properties of the emitted photons. (a) Angular distribution of all the emitted photons relative to the laser propagation axis (0°) at 1.5 ps in the cone-sandwich target; (b) Angular distribution of all the emitted photons relative to two-directional peak positions (∓150°) at 1.5 ps in the cone-plane target with a double-gaussian fitting function of $f(\theta) = a_1\exp[-\frac{(\theta-\theta_1)^2}{2\sigma_1^2}] + a_2\exp[-\frac{(\theta-\theta_2)^2}{2\sigma_2^2}]$. The divergence angle θ of the emitted photon is calculated as $\theta = \tan^{-1}(p_y/p_x)$ for each emitted photon; (c) The radiated photon energy as a function of the longitudinal momenta of the emitting fast electrons at 1.5 ps for the two targets; (d) The emitted photon energy spectrum snapshots at 1.5 ps for the cone-sandwich (red) and cone-plane (blue) target, respectively.

calculated the important generation points of the emitted photons, and their motions through the domain were not simulated and they stayed where they were generated. However, the absorption of the emitted photons by the target itself is an important issue. This is a must that we fabricated target in the real experiment. In fact, if we used plastic in the inner region (low density) for the cone-sandwich target, the density gradient will guide the fast electron transport and then the resultant high-directional photon emissions in this region. In this case, the transmission coefficient is greater than 99.5% and 95.6% for the photon's energy above 10 keV in 10 μm and 100 μm plastic target [36]. Therefore, the divergence angle distribution and energy spectrum of the emitted photons at the rear side of the target will not be influenced by the absorption of the target itself. To have a good understanding of the underlying mechanisms of the high-directional X-ray photon emission in our proposed target, we will focus on the acceleration and propagation mechanism of the laser-plasma-induced electrons in the following section.

3.3. *Influence of self-generated magnetic field in high-directional photon emissions*

Based on the previous discussions, high-collimated fast electrons propagating in the cone-sandwich target would be the main reason of the high-directional X-ray photon emissions, which enhances the synchrotron radiation positively. In general, for such overdense plasmas, the generated fast electrons can be collimated [37] through either the external magnetic field or the spontaneously self-generated magnetic field. As illustrated in Fig. 5(a) and (b), the results clearly show that the large quasi-static self-generated magnetic fields appear along the interfaces of the cone-sandwich target with density gradient, and the magnetic field is oriented to keep the fast electrons contained inside the middle transportation region at two different times. At 0.8 ps we found the magnetic field of 3.1157 kT (311 MG), which first appears at the region close to the laser-plasma interactions region. After that, the magnetic field continues to the rear side of the target due to the transportation of the fast electrons until 1.5 ps. Seen from the direction of magnetic fields along the interfaces of the density gradient, the fast electrons can be guided inside the middle transport region due to the imposed Lorentz force. This is also consistent with the guiding effects of the fast electrons in Fig. 2(a). After traveling through the target, although the fast electrons experience the obvious transverse oscillations driven by the laser's electric field, they are accelerated in the forward direction and confined by the self-generated magnetic filed into the middle transport channel. The deviation of the fast electrons induced by the magnetic field will enhance the high-directional photons in the transportation channel, and this can be certificated well by the emitted photon's number density profiles in Fig. 2(c). Contrarily, for the cone-plane target in Fig. 5(c) and (d), no quasi-static self-generated magnetic field is formed due to the uniform density distribution ($5n_c$). Therefore, after the fast electrons generation they are scattered almost in all

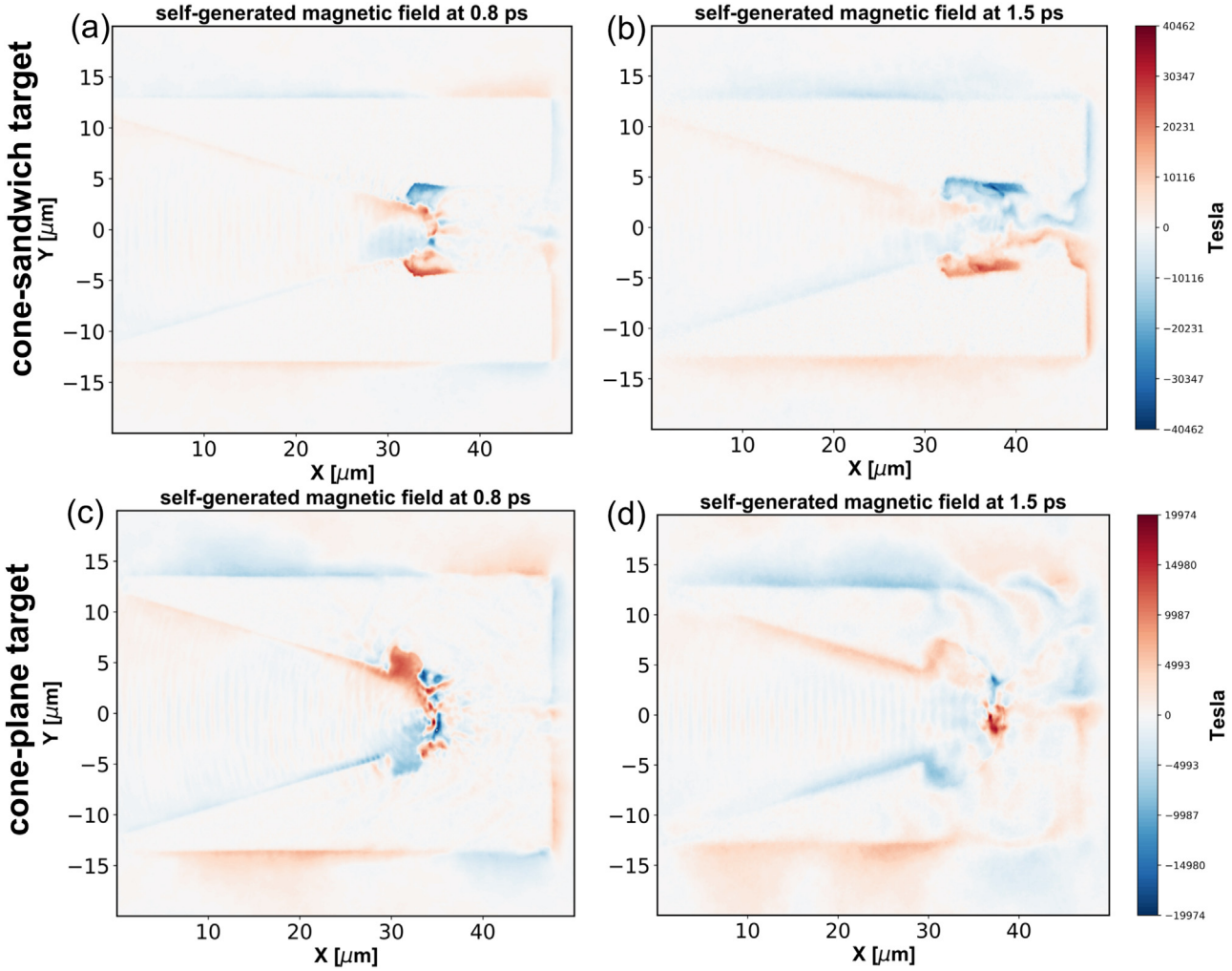

Fig. 5. Averaged z-component of the self-generated magnetic field B_z(T) along the interfaces of the density gradient at different times of (a) 0.8 ps and (b) 1.5 ps for the cone-sandwich target, and averaged B_z(T) snapshots at (c) 0.8 ps and (d) 1.5 ps for the cone-plane target.

directions as shown in Fig. 2(d) and Fig. 3(b).

Thus far, several mechanisms can induce a strong magnetic field generation in laser-plasma interactions, such as resistive jump [38,39] and anomalous resistivity [40]. The magnetic field generation induced by either the thermoelectric effect ($\partial \mathbf{B}/\partial t \propto \nabla n \times \nabla T$) with a temperature gradient, or the resistive material boundary $\partial \mathbf{B}/\partial t = c[\eta_r \nabla \times \mathbf{j}_f + \nabla \eta_r \times \mathbf{j}_f]$ with the collision effects. Here, $\mathbf{j}_f$ is the fast electron current density, and η_r is the material's resistivity. In the current case, the rapid magnetic field generation is produced by the density gradient which causes the rapid changing of the flow velocity of the background return electrons in the transverse direction. Since the laser pulse duration is longer than the plasma period, the plasma remains charge neutrality throughout the process during the fast electrons propagate the plasma target. In this case, a return current of background thermal electrons will be generated to neutralize the fast electrons everywhere according to the Alfvén current limit [41], except at the interfaces of different density regions within a skin depth. The self-generated magnetic field exists within a skin depth width near the interface of different regions, and can be expressed as the following formula [42]:

$$\frac{m_e c^2}{4\pi e^2}\nabla \times \left(\frac{\gamma \nabla \times \mathbf{B}}{n_e}\right) + \mathbf{B} = \frac{m_e \gamma c}{e^2}\left(\frac{1}{n_e}\nabla \times \mathbf{j}_f - \frac{1}{n_e^2}\nabla n_e \times \mathbf{j}_f\right), \tag{3}$$

where $\mathbf{j}_f$ is the fast electron current density, and γ is the relativistic factor of the fast electron. n_e denotes the number density of different regions in the target. From equation (3), the interplay of two effects will serve to illustrate the generation of collimating magnetic field in solid density region. The first right term induces a magnetic field which pushes the fast electrons to the region of higher fast electron current density, while the second term pushes the fast electrons towards the region of lower density. The theory predicts that the growth of the out of plane magnetic field at the interface between the two different fast electron current density regions, and the collimating self-generated magnetic field is expected to remain stable for the much longer pulses. This is also the reason why we adopted a longer laser pulse duration (1.5 ps) in our simulations. Supposing the number density of the middle transportation layer is lower than those of the top and bottom layers, then Eq. (3) gives the maximum self-generated magnetic field as the following [42]:

$$B_{\max} \approx \frac{m_e w_0}{e n_c}\frac{n_{f\_\mathrm{low}} v_{f\_\mathrm{low}}}{\sqrt{n_{\mathrm{low}}/n_c}} \approx 200\frac{\eta}{f}\frac{I_{18}^{0.5}\lambda_{\mu m}}{\sqrt{(n_{\mathrm{flow}} - n_{f\_\mathrm{low}})/n_c}}\frac{v_{f\_\mathrm{low}}}{c}\ (\mathrm{MG}), \tag{4}$$

where n_{low} is the electron density of the middle layer (lower density region), and I_{18} means the laser intensity in unites of 10^{18} W/cm^2. $n_{f\_\mathrm{low}} \approx 2\eta I_{18}^{0.5}\lambda_{\mu m}/f$ is the fast electron density in middle layer [43], and $2\eta/f$ is approximately 0.7072 at the higher laser intensity. v_{f_low} is the velocity of the fast electron. Using the initial target parameters and substituting them into Eq. (4), the maximum estimation of the self-generated magnetic field along the interfaces will be up to 292 MG. This

value is in good agreement with the peak value of magnetic field (311 MG) derived from the PIC simulations. In such an intense magnetic field, the Larmor radius ($\gamma_L(\mu m) \approx 30E_{MeV}/B_{MG}$) of the maximum fast electron energy extracted from PIC results (28.4 MeV shown in Fig. 3(d)) is approximately 2.74 μm. Thus, we expect significant guiding and collimation effects of fast electrons in the transport channel with low density (its radius of 5 μm in the target). Based on the above discussions, it is the self-generated magnetic field along the interface that guides most of the fast electrons propagating the middle transport region in the proposed target, and then it is the collimated fast electrons that radiates and enhances much higher-directional X-ray photons.

4. Conclusions

The current work aims at providing a high-directional laser-plasma X-ray emission source assisted by the collimated fast electrons in targets with a self-generated magnetic field, followed by the detailed discussions of the underlying mechanisms. We have investigated the photon emissions in the proposed cone-attached sandwich target with a number density gradient at a laser intensity of 2.5×10^{20} W/cm^2 by using PIC simulations. We have directly shown that most of the high-directional photon emissions are radiated by the forward-moving fast electrons, compared with the cone-plane target. Although these fast electrons will be experienced slightly transverse oscillations due to the electric field of the laser, they can be guided and confined by the resultant self-generated magnetic field along the interface of the proposed target with a sharp density gradient. The magnetic field is large enough to confine most of the fast electrons passing through the middle transport region with a small divergence angle. Additionally, the simulation results are consistent with the analytical model of the magnetic field generation. These findings indicate that it is the self-generated magnetic field along the interface that guides the fast electrons propagating the middle transport region, and also it is the collimating fast electrons that generates and enhances much higher-directional X-ray photon emissions. Along with the fast-developing laser and plasma diagnostic technologies, we expect that the high-directional and focused X-ray photon source has great potential applications in high energy density science, inertial confinement fusion, cancer therapy, material science, X-ray communication modulated source, and so forth.

Acknowledgements

We acknowledge support from the China Scholarship Council (CSC), the Fundamental Research Funds for the Central Universities (Grant No. NP2018408), the State Key Laboratory of Simulation and Effects of Intense Pulse Radiation Environment (SKLIPR1813), the Postgraduate Research & Practice Innovation Program of Jiangsu Province (Grant No. KYCX17_0257), the Special Foundation of China Postdoctoral Science Foundation (Grant No. 2018T110500), the Project supported by the Fundamental Research Funds for the Central Universities (Grant No. NP2018408), and the Priority Academic Program Development of Jiangsu Higher Education Institutions (PAPD). We appreciate the discussions about the EPOCH code which is developed under the UK EPSRC Grant Nos. EP/G054950/1, EP/G056803/1, EP/G055165/1 and EP/M022463/1.

References

[1] W. Kruer, The Physics of Laser Plasma Interactions, CRC Press, 2018.
[2] I.H. Hutchinson, Principles of plasma diagnostics, Plasma Phys. Control. Fusion 44 (2002) 2603.
[3] N. Lemos, F. Albert, J. Shaw, D. Papp, R. Polanek, P. King, A. Milder, K. Marsh, A. Pak, B. Pollock, et al., Bremsstrahlung hard X-ray source driven by an electron beam from a self-modulated laser wakefield accelerator, Plasma Phys. Control. Fusion 60 (2018) 054008.
[4] N. Fleurot, C. Cavailler, J. Bourgade, The laser megajoule (LMJ) project dedicated to inertial confinement fusion: development and construction status, Fusion Eng. Des. 74 (2005) 147–154.
[5] R. Tommasini, S. Hatchett, D. Hey, C. Iglesias, N. Izumi, J. Koch, O. Landen, A. MacKinnon, C. Sorce, J. Delettrez, et al., Development of Compton radiography of inertial confinement fusion implosions, Phys. Plasmas 18 (2011) 056309.
[6] C.P. Jones, C.M. Brenner, C.A. Stitt, C. Armstrong, D.R. Rusby, S.R. Mirfayzi, L.A. Wilson, A. Alejo, H. Ahmed, R. Allott, et al., Evaluating laser-driven bremsstrahlung radiation sources for imaging and analysis of nuclear waste packages, J. Hazard. Mater. 318 (2016) 694–701.
[7] B. Larson, W. Yang, G. Ice, J. Budai, J. Tischler, Three-dimensional X-ray structural microscopy with submicrometre resolution, Nature 415 (2002) 887.
[8] M.J. Berger, J. Hubbell, XCOM: Photon Cross sections on a Personal Computer, National Bureau of Standards, 1987 Technical Report.
[9] S. Bartzsch, U. Oelfke, Line focus X-ray tubes-a new concept to produce high brilliance X-rays, Phys. Med. Biol. 62 (2017) 8600.
[10] S. Hussain, M. Shafiq, R. Ahmad, A. Waheed, M. Zakaullah, Plasma focus as a possible X-ray source for radiography, Plasma Sources Sci. Technol. 14 (2005) 61.
[11] H. Li, X. Tang, S. Hang, Y. Liu, D. Chen, Potential application of X-ray communication through a plasma sheath encountered during spacecraft reentry into earth's atmosphere, J. Appl. Phys. 121 (2017) 123101.
[12] Y. Liu, H. Li, Y. Li, S. Hang, X. Tang, Transmission properties and physical mechanisms of X-ray communication for blackout mitigation during spacecraft reentry, Phys. Plasmas 24 (2017) 113507.
[13] S. Corde, K.T. Phuoc, G. Lambert, R. Fitour, V. Malka, A. Rousse, A. Beck, E. Lefebvre, Femtosecond X-rays from laser-plasma accelerators, Rev. Mod. Phys. 85 (2013) 1.
[14] G. Shvets, Laser-plasma accelerators: Gamma-rays going cheap, Nat. Phys. 7 (2011) 834.
[15] N.D. Powers, I. Ghebregziabher, G. Golovin, C. Liu, S. Chen, S. Banerjee, J. Zhang, D.P. Umstadter, Quasi-monoenergetic and tunable X-rays from a laser-driven Compton light source, Nat. Photon. 8 (2014) 28.
[16] L. Chen, W. Yan, D. Li, Z. Hu, L. Zhang, W. Wang, N. Hafz, J. Mao, K. Huang, Y. Ma, et al., Bright betatron X-ray radiation from a laser-driven-clustering gas target, Sci. Rep. 3 (2013) 1912.
[17] H. Li, X. Tang, S. Hang, Y. Liu, J. Mu, W. Zhou, Re-entry blackout elimination and communication performance analysis based on laser-plasma-induced X-ray emission, Phys. Plasmas 26 (2019) 033503.
[18] L. Ji, A. Pukhov, I.Y. Kostyukov, B. Shen, K. Akli, Radiation-reaction trapping of electrons in extreme laser fields, Phys. Rev. Lett. 112 (2014) 145003.
[19] D. Stark, T. Toncian, A. Arefiev, Enhanced multi-MeV photon emission by a laser-driven electron beam in a self-generated magnetic field, Phys. Rev. Lett. 116 (2016) 185003.
[20] T. Huang, A. Robinson, C. Zhou, B. Qiao, B. Liu, S. Ruan, X. He, P. Norreys, Characteristics of betatron radiation from direct-laser-accelerated electrons, Phys. Rev. E 93 (2016) 063203.
[21] K. Ledingham, W. Galster, Laser-driven particle and photon beams and some applications, N. J. Phys. 12 (2010) 045005.
[22] S. Kneip, S. Nagel, C. Bellei, N. Bourgeois, A. Dangor, A. Gopal, R. Heathcote, S. Mangles, J. Marques, A. Maksimchuk, et al., Observation of synchrotron radiation from electrons accelerated in a petawatt-laser-generated plasma cavity, Phys. Rev. Lett. 100 (2008) 105006.
[23] T. Arber, K. Bennett, C. Brady, A. Lawrence-Douglas, M. Ramsay, N. Sircombe, P. Gillies, R. Evans, H. Schmitz, A. Bell, et al., Contemporary particle-in-cell approach to laser-plasma modelling, Plasma Phys. Control. Fusion 57 (2015) 113001.
[24] L. Ji, A. Pukhov, E. Nerush, I.Y. Kostyukov, B. Shen, K. Akli, Energy partition, γ-ray emission, and radiation reaction in the near-quantum electrodynamical regime of laser-plasma interaction, Phys. Plasmas 21 (2014) 023109.
[25] C.P. Ridgers, J.G. Kirk, R. Duclous, T. Blackburn, C. Brady, K. Bennett, T. Arber, A. Bell, Modelling gamma-ray photon emission and pair production in high-intensity laser-matter interactions, J. Comput. Phys. 260 (2014) 273–285.
[26] R. Duclous, J.G. Kirk, A.R. Bell, Monte Carlo calculations of pair production in high-intensity laser-plasma interactions, Plasma Phys. Control. Fusion 53 (2010) 015009.
[27] A. Kemp, F. Fiuza, A. Debayle, T. Johzaki, W. Mori, P. Patel, Y. Sentoku, L. Silva, Laser-plasma interactions for fast ignition, Nucl. Fusion 54 (2014) 054002.
[28] Y. Sentoku, K. Mima, H. Ruhl, Y. Toyama, R. Kodama, T. Cowan, Laser light and hot electron micro focusing using a conical target, Phys. Plasmas 11 (2004) 3083–3087.
[29] Y. Sentoku, W. Kruer, M. Matsuoka, A. Pukhov, Laser hole boring and hot electron generation in the fast ignition scheme, Fus. Sci. Technol. 49 (2006) 278–296.
[30] H. Habara, G. Xu, T. Jitsuno, R. Kodama, K. Suzuki, K. Sawai, C. Barty, T. Kawasaki, H. Kitamura, K. Kondo, et al., Pulse compression using segmented grating in Gekko Mii system, ILE, J. Phys.: Conf. Ser. 112 (2008) 032017.
[31] Y. Ping, R. Shepherd, B. Lasinski, M. Tabak, H. Chen, H. Chung, K. Fournier, S. Hansen, A. Kemp, D. Liedahl, et al., Absorption of short laser pulses on solid targets in the ultrarelativistic regime, Phys. Rev. Lett. 100 (2008) 085004.
[32] T. Huang, C. Zhou, H. Zhang, S. Wu, B. Qiao, X. He, S. Ruan, Collimated gamma photon emission driven by pw laser pulse in a plasma density channel, Appl. Phys. Lett. 110 (2017) 021102.
[33] S. Palaniyappan, B.M. Hegelich, H.-C. Wu, D. Jung, D.C. Gautier, L. Yin, B.J. Albright, R.P. Johnson, T. Shimada, S. Letzring, et al., Dynamics of relativistic transparency and optical shuttering in expanding overdense plasmas, Nat. Phys. 8 (2012) 763.
[34] G. Malka, J. Miquel, Experimental confirmation of ponderomotive-force electrons produced by an ultrarelativistic laser pulse on a solid target, Phys. Rev. Lett. 77 (1996) 75.
[35] S. Cipiccia, M.R. Islam, B. Ersfeld, R.P. Shanks, E. Brunetti, G. Vieux, X. Yang, R.C. Issac, S.M. Wiggins, G.H. Welsh, et al., Gamma-rays from harmonically resonant betatron oscillations in a plasma wake, Nat. Phys. 7 (2011) 867.
[36] E. Gullikson, X-ray Interactions with Matter, (1995) http://www.henke.lbl.gov/

optical_constants/.
[37] P. McKenna, D. Neely, R. Bingham, D. Jaroszynski, Laser-Plasma Interactions and Applications, Springer, 2013.
[38] A. Robinson, M. Sherlock, Magnetic collimation of fast electrons produced by ultraintense laser irradiation by structuring the target composition, Phys. Plasmas 14 (2007) 083105.
[39] A. Robinson, M. Sherlock, P. Norreys, Artificial collimation of fast-electron beams with two laser pulses, Phys. Rev. Lett. 100 (2008) 025002.
[40] S. Wu, C. Zhou, S. Zhu, Effect of density profile on beam control of intense laser-generated fast electrons, Phys. Plasmas 17 (2010) 063103.
[41] H. Alfvén, On the motion of cosmic rays in interstellar space, Phys. Rev. 55 (1939) 425.
[42] H.B. Cai, S.P. Zhu, M. Chen, S.Z. Wu, X. He, K. Mima, Magnetic-field generation and electron-collimation analysis for propagating fast electron beams in overdense plasmas, Phys. Rev. E 83 (2011) 036408.
[43] A. Bell, A. Robinson, M. Sherlock, R. Kingham, W. Rozmus, Fast electron transport in laser-produced plasmas and the KALOS code for solution of the Vlasov–Fokker–Planck equation, Plasma Phys. Control. Fusion 48 (2006) R37.